Oxygen adsorption on the Al9Co2(001) surface: first-principles and STM study

Sebastian Alarcon Villaseca, Laura Serkovic Loli, Julian Ledieu, Vincent Fournée, Peter Gille, Jean-Marie Dubois, Emilie Gaudry

HAL Id: hal-00977985
https://hal.science/hal-00977985

Submitted on 20 Oct 2014

Oxygen adsorption on the Al_9Co_2(001) surface: first-principles and STM study

S. Alarcón Villaseca[1], L.N. Serkovic Loli[1], J. Ledieu[1], V. Fournée[1], P. Gille[2], J.-M. Dubois[1] and É. Gaudry[1]

[1] Institut Jean Lamour, UMR 7198 (CNRS Université de Lorraine), Parc de Saurupt, 54011 Nancy Cedex, France. [2] Department of Earth and Environmental Science, Crystallography Section, LMU, Theresienstr. 41, D-80333 München, Germany.

E-mail: `Emilie.Gaudry@ijl.nancy-universite.fr`

Abstract. Atomic oxygen adsorption on the pure aluminium terminated Al_9Co_2(001) surface is studied by first principle calculations coupled with STM measurements. Relative adsorption energy of oxygen atoms have been calculated on different surface sites along with the associated STM images. The local electronic structure of the most favourable adsorption site is described. The preferential adsorption site is identified as a "bridge" type site between the cluster entities exposed at the (001) surface termination. The Al-O bonding between the adsorbate and the substrate presents a covalent character, with $s-p$ hybridization occuring between the states of the adsorbed oxygen atom and the aluminium atoms of the surface. The simulated STM image of the preferential adsorption site is in agreement with experimental observations. This work shows that oxygen adsorption generates important atomic relaxations of the topmost surface layer and that sub-surface cobalt atoms strongly influence the values of the adsorption energies. The calculated Al-O distances are in agreement with those reported in Al_2O and Al_2O_3 oxides and for oxygen adsorption on Al(111).

1. Introduction

Aluminium-based oxide barriers are widely used in the manufacture of stable coatings which are typically resistant to high temperature and corrosive environments [1]. These oxide barriers are also at the origin of the loss of performance of heterogeneous catalysts working during long term exposition under real industrial conditions [2]. From these two examples, the study of the interaction of oxygen with metallic surfaces appears vital in the comprehension of a broad range of chemical processes of technological relevance.

The low resistance of metallic surfaces towards oxidation is related to the strong negative values of the enthalpies of formation of the oxides, e.g. for the oxide Al_2O_3 the enthalpy of formation is ΔH_f = -1675 kJ/mol, which means that oxide phases are energetically more favourable [2, 3]. The oxidation of a metallic surface is a complex phenomenon that involves different steps. In a general way, it has been established that the first step of surface oxidation is the dissociation of the adsorbed O_2 molecules. Experimentally, measurements of the probability of dissociation show that the O_2 molecule dissociates on metallic surfaces [4, 5]. Here, the reaction yield of the dissociative reaction increases with the kinetic energy up to saturation at $\simeq$ 0.6 eV [4, 5]. This process is followed by the adsorption of the dissociated oxygen atoms on the substrate, which form strong bonds with the atoms at the surface [4]. In a high number of metallic surfaces, the preferential adsorption sites typically correspond to atomic surface environments of symmetry 3 or 4, referred to hollow sites. The sticking probability (P_S) of an oxygen atom on the surface of a metal is high, e.g. at 300 K P_S is of the order of 1 for Ni and Co [3]. Surface dissociation and penetration of oxygen in the sub-surface of the solid may also occur and they can generate reconstructions of the surface atomic structure as well as the formation of an oxide phase in the topmost layers [4]. Similar to the pure aluminium surfaces, oxygen adsorption on the surfaces of Al-TM (TM = transition metal) alloys generally leads to the formation of Al_2O_3 oxide layers in the surface. The latter is related to the larger stability of the Al_2O_3 oxide compared to the transition metal oxides [1]. Oxygen adsorption on the (100) surface of the equi-atomic AlCo intermetallic compound allows to illustrate this point. In the study of V. Rose *et al.* [6], it is demonstrated that the formation at 300 K of an Al_2O_3 layer is thermodynamically more favourable (ΔH_f = -1675 kJ/mol) than the formation of the CoO (ΔH_f = -238 kJ/mol) and Co_3O_4 (ΔH_f = -891 kJ/mol) oxides. This study also shows that the AlCo(100) surface is completely covered by amorphous Al_2O_3 [6]. The situation is similar in the low-index surfaces of the AlNi, $AlNi_3$, GaCo and AlFe alloys: the formation of an Al_2O_3 (Ga_2O_3) layer is favoured [7, 8, 9].

One of the most widely used methods to determine the adsorption sites of oxygen atoms in metallic surfaces is scanning tunnelling microscopy (STM). Nevertheless, the interpretation of the experimentally recorded STM images is delicate. Even in the simple case of O_2 adsorption on a Al(111) surface, fundamental questions remain open, particularly regarding the dissociation process of the O_2 molecule [10, 11]. The work of H. Brune *et al.* [12, 13] show that atomic oxygen on Al(111) appear at dark contrast in

STM images recorded at room temperature. It is attributed to the presence of atomic oxygen in fcc sites. Moreover, it is claimed that the distance of separation between both atoms of a dissociated O$_2$ molecule at room temperature on the Al(111) surface is of the order of 80 Å. The authors called this effect "surface migration of hot adatoms" [12, 13]. Later studies demonstrated that the oxygen atoms from a dissociated O$_2$ molecule were diffusing distances of 2 or 3 times the surface lattice parameter, with a distance of separation of about 10-15 Å [4, 10, 11, 14, 15]. In the work of M. Schmid *et al.* [10], the dark contrast observed in STM images was attributed to groups of atoms on the surface, i.e. dimers, trimers, etc. Differences with previous works were explained by the interaction between the STM tip and the sample. At lower temperatures (80 K), the STM images show the presence of dark contrast forming pairs of black dots [10]. Some of these dark dots are sometimes lengthened according to the low index directions of the surface and they are interpreted as pairs of oxygen atoms, placed each one in adjacent fcc hollow sites. Nevertheless, the STM images also show pairs of black dots for which neither the direction nor the distance of separation are compatible with two oxygen atoms occupying fcc sites [10]. So far, several models have been elaborated to explain these observations. One model involves oxygen atoms negatively charged that describe ballistic trajectories [4]. A second model has been proposed to attribute a different role to the two dissociated oxygen atoms: one of the atoms of the O$_2$ molecule forms a bond with the surface and the other atom is ejected ("canon ball motion") [10]. These examples show that even in simple cases, like the dissociation of the O$_2$ molecule on the Al(111) surface, the interpretation of STM images recorded during the oxygen adsorption is not straightforward, partly because STM images are linked to the electronic structure of the surface and do not image directly the atomic positions of the surface atoms. In the case of alloys, the understanding of the oxidation process is expected to show similar trends: generally the adsorbed oxygen atoms appear as depressions in the STM images (dark contrast) [6, 8, 9, 16, 17, 18]. For example, in the oxidation of the PdAg(111) surface, the clear contrast zones observed in the STM images of the clean surface correspond to palladium atoms, which become dark in response to the adsorption of atomic oxygen [16]. This can be interpreted as a selective adsorption of oxygen atoms on Pd sites isolated by Ag atoms [16].

The study of the oxidation of metallic surfaces constitutes a challenge in surface science, since the interaction between a surface and an adsorbate can induce important structural modifications under ultra high vacuum conditions [2]. To understand the mechanisms of the different steps towards oxide surface formation, an analysis at atomistic scale is essential. An approach combining experimental STM analysis and first-principles STM images, simulated from model structures within the Tersoff-Hamann approximation [19, 20], represents a powerful tool to study the first steps of the oxidation. In this article, we focus on the adsorption of atomic oxygen on the (001) surface of the intermetallic compound Al$_9$Co$_2$. The Al$_9$Co$_2$ crystal is an intermetallic with an intermediate structural complexity between the *B*2-AlCo and the decagonal Al-Ni-Co quasicrystal. Al-based intermetallic compounds have been attracting great

research interest regarding applications, since they combine good mechanical properties and low density [21, 22, 1, 23, 24]. As a complex metallic alloy, the electronic structure of Al$_9$Co$_2$ includes a pseudogap near the Fermi energy [25], which suggests that this material could present a superior corrosion resistance, like quasicrystals, compared to simpler alloys [26, 27, 28, 29]. The (001) surface is bulk truncated, with the selection of a pure aluminium layer as terminating plane. Although the topmost layer is a pure aluminium termination, the sub-layer contains cobalt atoms that can play an important role in the adsorption properties and reactivity of the surface.

The paper is organized as follows. Calculations and experimental details are gathered in section 2. The identification of the most favoured adsorption sites, the analysis of the bonding between atomic oxygen and the surface and the confrontation of the theoretical results with experimental observations are presented and discussed in section 3 before we conclude.

2. Calculation and experimental details

2.1. Calculation details

Calculations are performed using the Vienna ab initio Simulation Package (VASP) based on the Density Functional Theory (DFT) [30, 31]. The interaction between the valence electrons and the ionic core is described using the projector-augmented wave (PAW) method [32, 33]. The electronic exchange and correlation contribution is described using the generalized gradient approximation GGA-PBE [34, 35]. Geometries are optimized by the calculation of the Hellmann-Feynman forces acting on atoms and their minimization via a conjugate gradient algorithm. The parameters linked to the numerical implementation of the DFT, i.e. the plane-wave cutoff E_{cut} and the density of k-points sampling the Brillouin zone, were converged by means of a series of test calculations on bulk Al$_9$Co$_2$ (22 at/cell). The chosen values for E_{cut} (350 eV) and the size of the Monkhorst-Pack k-points mesh (8x8x8) achieve a precision for the bulk total energy smaller than 4 meV. For the calculations using slabs, we keep an identical k-grid mesh (8x8x1).

The optimization of the bulk structure of the intermetallic compound Al$_9$Co$_2$ and the atomic structure model of the (001) surface has been fully described in reference [25]. Adsorption of atomic oxygen is simulated by building non-symmetric slabs separated by a 20 Å-thick vacuum region, where the position of the oxygen atom is relaxed starting from a 3 Å distance above the surface site. Based on the results of Baker *et al.* [36, 37], it has been considered that the 20 Å-thick vacuum region is sufficient to ensure that the dipolar effect induced by the adsorbed oxygen atom on one side of the slab will not produce any important calculation artefact. Eleven-layer-thick slabs are used to perform the present study: the 5 atomic layers at the bottom are kept fixed while the other 6 top layers are allowed to fully relax (surface of interest). As shown in our previous study [25], this configuration is sufficient to obtain both accurate electronic and atomic

structures. A comparison between the values of the relative adsorption energies obtained for different adsorption sites (which will be discussed in section 3.1) within an 11-layer-thick slab and a 6-layer-thick slab shows contrasted differences: it is smaller than 40 meV for the bridge type sites B_1, B_2 and B_3, but of the order of 200 meV for the sites T_1 and H_2 (see figure 1a). In the paper, we use a 1x1 surface unit cell. A comparison using a 2x2 surface unit cell indicates that the adsorption energy differences are small (smaller than 20 meV) for the considered adsorption sites (B_1, B_2, B_3 and H_2). Our calculations were performed without taking into account spin-polarization effects on the obtained total energies. We have nevertheless verified that for different adsorption sites (namely B_2 and B_3, using a 6 layer thick slab with 2x2 surface unit cell), the total energy differences between calculations with and without spin-polarization are smaller than 1 meV.

2.2. Experimental details

The preparation of the Al$_9$Co$_2$(001) surface consists of repeated cycles of Ar$^+$ ion sputtering for 30 minutes followed by annealing at different temperatures ranging from 843 to 1043 K, all of this under ultra high vacuum conditions (base pressure 5x10^{-11} mbar, see Ref. [25] for more details). The temperature has been measured using an infrared optical pyrometer with the emissivity set to 0.35. To check the cleanliness and the overall structure of the surface, x-ray photoelectron spectroscopy (XPS) and low electron energy diffraction (LEED) have been used. The local atomic structure was investigated by STM (tungsten tip) and the electronic structure of the surface has been measured at room temperature using ultraviolet photoelectron spectroscopy (UPS) and scanning tunnelling spectroscopy (STS).

3. Results and discussion

3.1. Identification of the most favoured sites for atomic oxygen adsorption

The adsorption sites considered in this study are labelled Top (T), Hollow (H) and Bridge (B), with 1-fold, 4-fold and 2-fold symmetry respectively. In the case of a T_i site (where index $i = 1$ to 2 labels all T sites considered in this study), the adsorbed atom is lying over one Al atom in the substrate. In the case of a B_j site (where index $j = 1$ to 3 labels all B sites considered in this study), the adsorbed atom forms a bridge between two Al atoms in the substrate, while in the case of a H_k site (where index $k = 1$ to 2 labels all H sites considered in this study) the adsorbed atom is located in between four Al substrate atoms (see Fig. 1). The chosen sites are exhaustive for the studied surface termination and they present different local surface stoichiometries, i.e. with differences in the atomic chemical environment around the adsorption site. The aim of the present selection of the adsorption sites is to determine which are the parameters acting on the first steps of the oxidation of the Al$_9$Co$_2$(001) surface. The relative adsorption energies

$\Delta E^{(i)}$, for different adsorption sites i, are evaluated according to the equation:

$$\Delta E^{(i)} = E_{Slab+O}^{(i)} - E_{Slab+O}^{B_3} \tag{1}$$

where $E_{Slab+O}^{(i)}$ is the total energy of the substrate-adsorbate system (slab + adsorbed oxygen atom in the site i) and $E_{Slab+O}^{B_3}$ the total energy of the slab plus the oxygen atom adsorbed in the B_3 site.

Figure 1(a) presents the different adsorption sites considered in this study as well as the relaxed final positions of the oxygen atoms. Their corresponding relative adsorption energies are presented in Table 1. The most favourable adsorption site corresponds to the B_3 site (with a total adsorption energy of -7.20 eV with respect to the free oxygen atom, consitent with the atomic oxygen adsorption energy on Al(111) [38, 39, 15]) followed by the H_1' site. Both sites are bridge sites. The site B_3 is also located between the cluster structures of the (001) surface termination (see Figure 1(b)). The adsorption energies of the B_2, B_1 and T_1' sites are calculated to be about 0.4 eV higher than the one of the B_3 site. The H_2, H_2' and T_1 sites are found the less favourable sites. The oxygen atoms initially positioned in H_1 (equivalent to H_3), T_1 and T_2 (equivalent to T_3) relax towards B_3, whereas the atoms initially located on the sites B_1, B_2 and B_3 present only small relaxations. An oxygen atom initially deposited in H_2 relaxes out of the centre of the site (site H_2').

The oxygen atoms adsorbed on the surface show a tendency to relax towards adsorption sites leading to Al-O distances close to the one determined for oxygen adsorbed on Al(111) (1.73 - 1.84 Å [40]) and similar to Al-O distances observed in Al$_2$O (1.70 Å [40]) and Al$_2$O$_3$ (1.86 Å [41]) oxides. The Al-O distance calculated for oxygen atoms located in the B_3 site is 1.75 Å. Oxygen atoms adsorbed on the T_1', H_2' and H_1' sites cause important relaxations of the surface aluminium atoms (Figures 1(c-e)): surface aluminium atoms rearrange around the adsorbed oxygen atom so that the latter, which was initially deposited in a 4-fold symmetry site, is finally located in a 3-fold symmetry site formed by 3 Al surface atoms. In the less favourable site (H_2), the Al-O distance is 1.92 Å.

The adsorption energies depend strongly on the Co-O distance. The most favourable adsorption site (B_3) is also the one that presents the largest Co-O separation (3.95 Å). In the less favourable site (H_2), the oxygen atom is relatively close to a cobalt atom (2.73 Å). The relative adsorption energy of the H_2' site is unfavourable, the oxygen atom is positioned almost over a sub-surface cobalt atom. In general, we can conclude that a large Co-O distance correlates with a more favourable adsorption site.

3.2. Electronic structure of the adsorbate-substrate system: site B_3

Figure 2 shows the local electronic density of states (LDOS) calculated for the surface before and after atomic oxygen adsorption. The effects of adsorption on the surface DOS are confined to the first two atomic layers (see Figure 2(left)). In the surface atomic
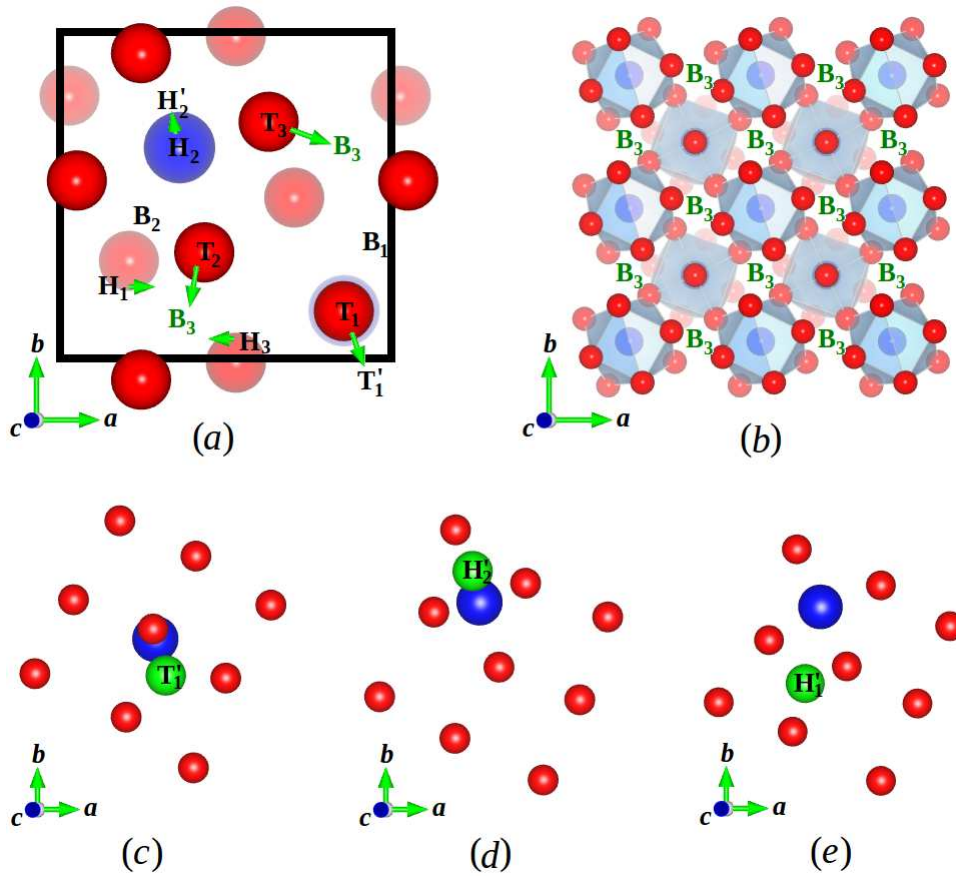
Figure 1. (a) Initial and final positions of the oxygen atoms adsorbed on the $Al_9Co_2(001)$ surface (top view, 1x1 surface unit cell represented in a black box). Red (blue) spheres represent the aluminium (cobalt) atoms. Sub-surface atoms appear hazed. The most important relaxations are indicated by green arrows and the most favourable adsorption site, B_3, is highlighted in green. (b) Cluster representation of the atomic structure of the $Al_9Co_2(001)$ surface. Substrate relaxations after atomic oxygen adsorption on the $Al_9Co_2(001)$ surface forming sites with almost 3-fold symmetry are shown for sites T_1' (c), H_2' (d) and H_1' (e). The blue sphere indicates the position of the nearest Co atom to the adsorbed oxygen atom (green spheres).

layers S and S-1, the corresponding structure of the DOS after adsorption differs from the DOS of the clean surface. Figure 2(middle) shows the details of the local DOS of the topmost surface atomic layer S, as well as the contributions of the surface aluminium atoms and the adsorbed oxygen atom. Figure 2(right) shows a certain number of common structures between the partial electronic DOS of the substrate surface and the adsorbed oxygen atom (between the Fermi energy and -6 eV). Particularly, common peaks are observed at energies of -5.9 eV and -3.8 eV, -2.7 eV, -1.0 eV and -0.4 eV. This strong mixing of the two sets of electronic states is characteristic of a covalent interaction, resulting in the hybridization between the electronic s-p states of the surface and the electronic s-p states of the oxygen atom. Furthermore, in the LDOS of the clean surface of Figure 2(right), a peak at -2.0 eV is observed. This particular peak disappears after the adsorption of the oxygen atom. In the clean surface, this structure is due to the

Table 1. Relative adsorption energies $\Delta E^{(i)}$ of the different adsorption sites considered in the study.

Initial Site	Final Site	$\Delta E^{(i)}$ [eV]
B_1	B_1	0.40
B_2	B_2	0.34
B_3	B_3	0.00
H_1	H_1' (near B_3)	0.17
H_2	H_2'	0.73
H_2	H_2	0.89
T_1	T_1'	0.45
T_1	T_1	0.90
T_2	B_3	0.00

hybridization between s-p states of the surface aluminium atoms and d states of the underlying sub-surface cobalt atom. It is possible to assume that the disappearance of this structure after the oxygen adsorption is due to the formation of an Al-O bond.
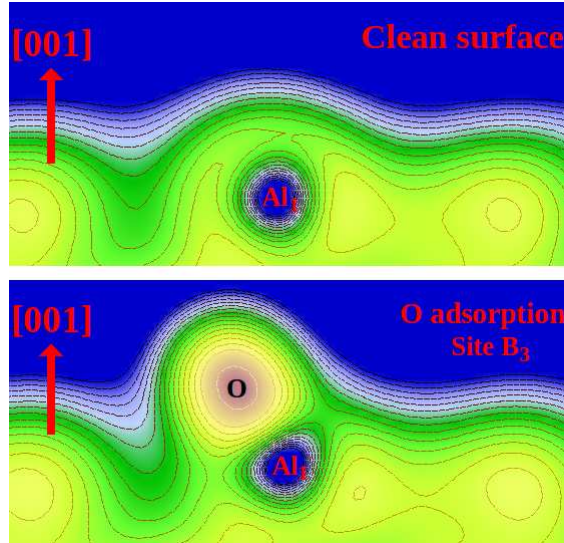
Figure 3 shows the charge density distribution of the adsorbed oxygen atom and one of the two aluminium atoms composing the B_3 site (the situation is the same for both Al atoms composing the B_3 site). In agreement with the previous findings, a non-uniform shape of the charge density is observed after oxygen adsorption. The deviation from spherical distribution of the charge density embedding the atoms point towards the formation of a covalent and directional bonding between the surface Al atoms and the adsorbed O atom, since the flattening of the charge density occurs in between these atoms.

3.3. Comparison between calculations and experimental observations by STM

Figure 4(a) shows an experimental STM image recorded at 300 K after adsorption of molecular oxygen on the Al₉Co₂(001) surface. Particularly, this STM image shows the substrate lattice as well as adsorbates with three different types of contrasts: (a) dark squares with a bright centre, (b) dark zones, and (c) bright dots. The number of motifs of type "b" and "c" increases with O₂ exposure while the number of motifs "a" remains constant. These assessments are deduced after the analysis of the experimental STM images, by measuring the areas of the image covered by motifs of type "a", "b" and "c" as a function of the O₂ dosage (Fig. 4(b)). Motifs of type "a" can already be observed on the bare substrate before O₂ exposure, and do not present any mobility. Therefore, we assume that type "a" corresponds to impurities or vacancies already present on the sample surface. Analysing consecutive STM scans recorded over the same region, it has been observed that several "c" motifs apparently disappear to be replaced by "b" motifs at the same site. At this stage, it is not clear if these "c" motifs diffuse across terraces between scans or transform into "b" motifs. For a limited number of cases, "c" motifs
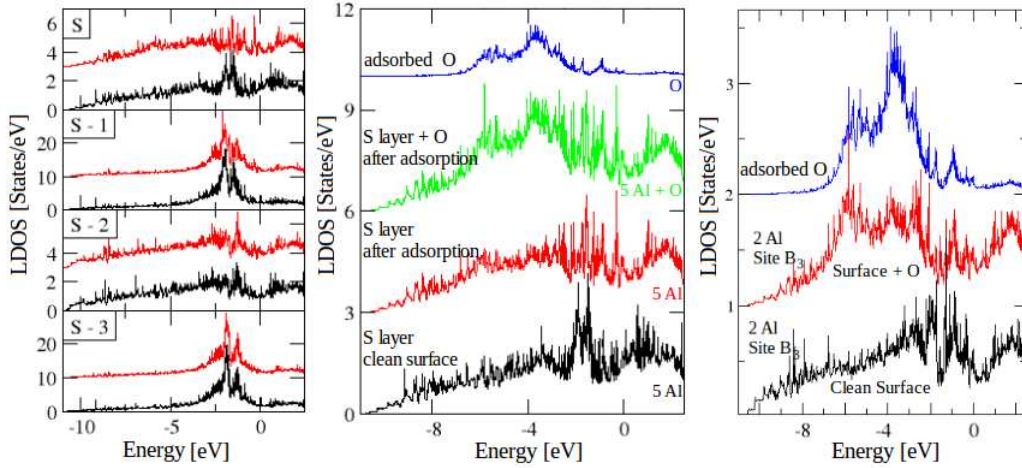
Figure 2. Left: Electronic LDOS structure of the atomic layers of the clean surface (black) and of the slab after atomic oxygen adsorption (red, site B_3); Middle: Different contributions to the electronic structure of the surface plane S (5 aluminium atoms per surface unit cell) and the adsorbed oxygen atom (B_3 site). Right: Partial LDOS (i) of the two Al atoms composing the B_3 site (black, clean surface), (ii) of the two Al atoms of the B_3 site after oxygen adsorption (red), (iii) of the adsorbed oxygen atom in the B_3 site (blue).

Figure 3. Slice cuts of the charge density distribution of the site B_3, composed of two Al atoms (only one shown), before (clean surface) and after atomic oxygen adsorption.

have appeared on top of already existing "b" motifs. These observations are consistent with the dissociative adsorption of O_2 molecules at the surface, the "b" and "c" motifs corresponding to oxygen atoms and/or O_2 molecules adsorbed on the surface.

Figure 5 presents the STM images that were simulated using the Tersoff-Hamann approximation [19, 20] for the adsorption of atomic oxygen in the H_2, H_1', B_3 and T_1 sites. The simulated images corresponding to the adsorption of oxygen in H_2 and T_1

(a)   (b)
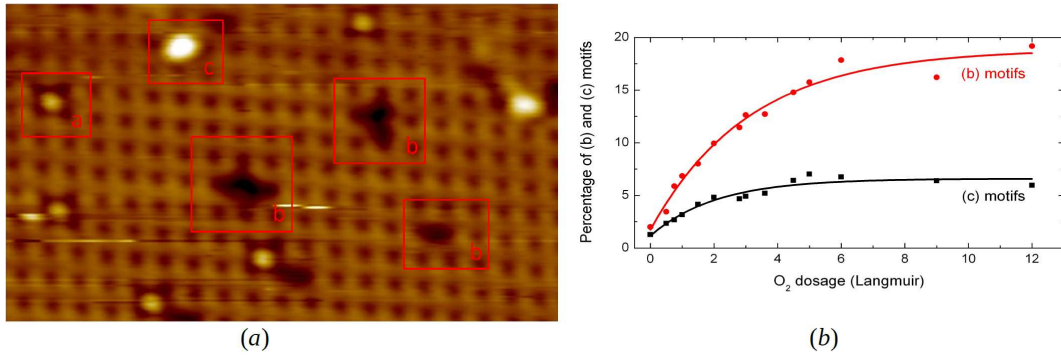
Figure 4. (a) Experimental STM image recorded at 300 K for an exposure of 0.5 Langmuir of O_2 deposition (9.6 x 12.1 nm^2, V_{bias} = -2 V). Red boxes identify the different motifs "a", "b" and "c" observed in the STM image. (b): Percentage of "b" and "c" motifs observed after O_2 dosage (in Langmuir).

sites show a bright point, that does not necessarily correspond to the position of the adsorbed atomic oxygen (red arrow on Fig. 5). From an energetic point of view, the sites H_2 and T_1 are not favourable, and the relative position of the bright spot with respect to the underlying pattern of the bare surface is different for the experimental and the simulated STM images. The motifs of type "c" might rather correspond to molecular oxygen adsorption, but precise determination of this point requires further studies. The simulated STM images corresponding to the adsorption of oxygen in site B_3 or H'_1 shows large dark areas, similarly to motif "b" of the experimental image. In addition, these two sites are the most favourable from an energetic point of view. This might allow us to interpret the motif "b" on the experimental STM image as the presence of atomic oxygen adsorbed in site B_3 or H'_1.
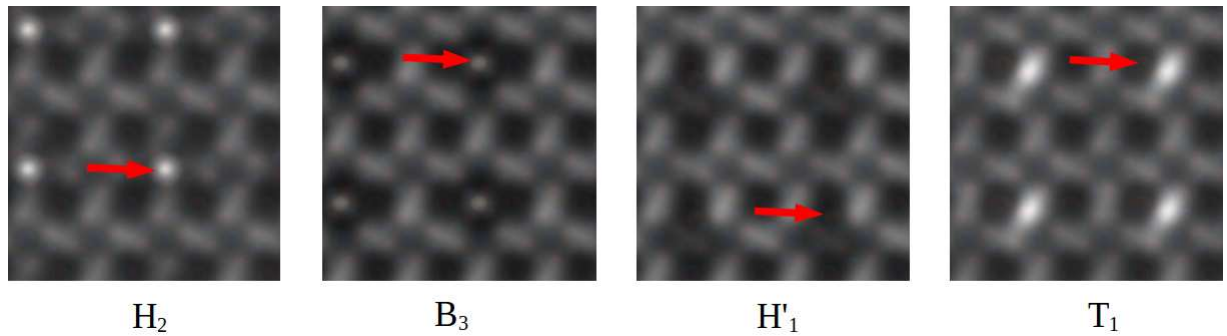
H_2 B_3 H'_1 T_1

Figure 5. Simulated STM images of the atomic oxygen adsorption on the H_2, B_3, H'_1 and T_1 sites. The tip-surface distance is 4 Å and V_{bias} = -1.3 V (2x2 surface unit cell). The red arrow show the position of the adsorbed oxygen atom.

4. Conclusions

In this article, the atomic oxygen adsorption on the (001) surface of the Al$_9$Co$_2$ intermetallic compound has been studied by means of calculations based on the DFT framework and experimental STM images. The preferential adsorption site has been identified as a bridge-type site between the cluster structures of the (001) surface termination (site B_3) and equidistant from the sub-surface Co atoms. The Al-O bonding between adsorbate and substrate shows a covalent behaviour, with hybridization between the oxygen s-p states and the aluminium s-p states of the surface. The simulated STM image from a slab containing one adsorbed oxygen atom in the preferential adsorption site presents a dark contrast in agreement with what is observed in the experimental STM images. In this study, it has also been shown that the oxygen adsorption generates important atomic relaxations of the topmost layer of the surface: oxygen atoms cause a rearrangement of the initial 4-fold sites, turning them into 3-fold sites. It has also been found that only weak relaxations are obtained when the oxygen atom is adsorbed on a bridge site: the adsorbed oxygen atoms suffer almost no relaxation in the directions parallel to the surface.

Finally, this work has shown that sub-surface cobalt atoms are found to strongly influence the values of the adsorption energies: the most favoured sites lie at the longest Co-O distances ($\simeq 3.95$ Å). Al-O distances are rather short in comparison with Co-O distances. When adsorbed in B_3 site, the Al-O distance is the smallest one ($\simeq 1.75$ Å). The obtained Al-O distances are in agreement with the typical distances of oxygen adsorption on the Al(111) surface, as well as with the Al-O distances in the Al$_2$O and Al$_2$O$_3$ oxides. Therefore, the formation of these oxides is expected on the (001) surface of the Al$_9$Co$_2$ compound. From our experimental results, these oxides would be disordered since the LEED pattern disappears when a rate of 17 langmuirs of O$_2$ is deposited on the surface at 300 K.

5. Acknowledgements

6. References

[1] E. Belin-Ferré, editor. *Surface properties and engineering of complex intermetallics*, volume 3. World Scientific Publishing, Singapore, 2010.

[2] K. Reuter, C. Stampfl, M.V. Ganduglia-Pirovano, and M. Scheffler. Atomistic description of oxide formation on metal surfaces: the example of ruthenium. *Chem. Phys. Letters*, 352:311, 2002.

[3] R.W. Joyner and R.A. Van Santen, editors. *Elementary Reaction Steps in Heterogeneous Catalysis.* NATO ASI. Series C, Kluwer Academic Pub., Dordrecht, 1993.

[4] G. Katz, R. Kosloff, and Y. Zeiri. Abstractive dissociation of oxygen over Al(111): A nonadiabatic quantum model. *J. Chem. Phys.*, 8:3931, 2004.

[5] L. Osterlund, I. Zoric, and B. Kasemo. Dissociative sticking of O$_2$ on Al(111). *Phys. Rev. B*, 55:15452, 1997.

[6] V. Rose, V. Podgursky, I. Costina, and R. Franchy. Growth of ultra-thin amorphous Al$_2$O$_3$ films on CoAl(100). *Surf. Sci.*, 541:128, 2003.

[7] V. Rose, V. Podgursky, I. Costina, R. Franchy, and H. Ibach. High temperature oxidation of CoAl(100). *Surf. Sci.*, 577:139, 2005.

[8] R. Franchy. Growth of thin, crystalline oxide, nitride and oxynitride films on metal and metal alloy surfaces. *Surf. Sci. Report*, 38:199, 2000.

[9] G. Schmitz, M. Eumann, D. Stapel, and R. Franchy. Combined EELS STM study of the adsorption of nitric oxide and the formation of GaO$_x$N$_y$ on CoGa(001). *Surf. Sci.*, 91:427, 1999.

[10] M. Schmid, G. Leonardelli, R. Tscheliessnig, A. Biedermann, and P. Varga. Oxygen adsorption on Al(111): low transient mobility. *Surf. Sci.*, 478:355, 2001.

[11] C. Carbogno, J. Behler, K. Reuter, and A. Gross. Signatures of nonadiabatic O$_2$ dissociation at Al(111): First-principles fewest-switches study. *Phys. Rev. B*, 81:035410, 2010.

[12] H. Brune, J. Wintterlin, R.J. Behm, and G. Ertl. Surface migration of hot adatoms in the course of dissociative chemisorption of oxygen on Al(111). *Phys. Rev. Lett.*, 68:624, 1992.

[13] H. Brune, J. Wintterlin, J. Trost, G. Ertl, J. Wiechers, and R.J. Behm. Interaction of oxygen with Al(111) studied by scanning tunnelling microscopy. *J. Chem. Phys.*, 99:2128, 1993.

[14] G. Wahnstrom, A.B. Lee, and J. Stromquist. Motion of "hot" oxygen adatoms on corrugated metal surfaces. *J. Chem. Phys.*, 105:326, 1996.

[15] Y. Yourdshahyan, B. Razaznejad, and B.I. Lundqvist. Adiabatic potential-energy surfaces for oxygen on Al(111). *Phys. Rev. B*, 65:075416, 2002.

[16] R. Wiesendanger and H.-J. Güntherodt, editors. *Scanning Tunneling Microscopy III.* Springer series in Surface Science 29, Springer Verlag, Berlin, 1993.

[17] W.A. Hofer. Challenges and errors: interpreting high resolution images in scanning tunneling microscopy. *Prog. Surf. Sci.*, 71:147, 2003.

[18] J.M. Blanco, F. Flores, and R. Prez. STM-theory: Image potential, chemistry and surface relaxation. *Prog. Surf. Sci.*, 81:403, 2006.

[19] J. Tersoff and D. R. Hamann. Theory and application for the scanning tunneling microscope. *Phys. Rev. Lett.*, 50:1998, 1983.

[20] J. Tersoff and D. R. Hamann. Theory of the scanning tunnelling microscope. *Phys. Rev. B*, 31:805, 1985.

[21] E. Belin-Ferré, editor. *Basics of Thermodynamics And Phase Transitions In Complex Intermetallics*, volume 1. World Scientific Publishing, Singapore, 2008.

[22] E. Belin-Ferré, editor. *Properties and Applications of Complex Intermetallics*, volume 2. World Scientific Publishing, Singapore, 2009.

[23] E. Belin-Ferré, editor. *Mechanical Properties of Complex Intermetallics*, volume 4. World Scientific Publishing, Singapore, 2010.

[24] K. H. J. Buschow, R. W. Cahn, M. C. Flemings, B. Ilschner, E. J. Kramer, Subhash Mahajan, and P. Veyssire, editors. *Encyclopedia of Materials: Science and Technology.* Elsevier Science Ltd., NY, 2001.

[25] S. Alarcón Villaseca, J. Ledieu, L.N. Serkovic Loli, M.-C. de Weerd, P. Gille, V. Fournée, J.-M. Dubois, and É. Gaudry. Structural investigation of the (001) surface of the Al$_9$Co$_2$ complex metallic alloy. *J. Phys. Chem. C*, 115:14922, 2011.

[26] D. Plachke, A. Khellaf, and H.D. Carstanjen. Initial oxidation of AlPdMn quasicrystals a study by high-resolution RBS and ERDA. *Nuclear Instruments and Methods in Physics Research B*, 190:646, 2002.

[27] D. Plachke, A. Khellaf, M. Kurth, A. Szokefalvi-Nagy, and H.D. Carstanjen. Initial oxidation of quasicrystals an investigation by high-resolution RBS and ERDA. *Journal of Non-Crystalline Solids*, 334-335:524, 2004.

[28] A. Lekatou, A.K. Skas, A.E. Karantzalis, and D. Sioulas. Microstructure and corrosion performance of Al-32%Co alloys. *Corrosion Science*, 63:193, 2012.

[29] A.I. Goldman, D. Sordelet, P. A. Thiel, and J. M. Dubois, editors. *New Horizons in Quasicrystals: Research and Applications.* World Scientific Publishing Co, Singapore, 1997.

[30] G. Kresse and J. Furthmüller. Efficient iterative schemes for ab initio total-energy calculations using a plane-wave basis set. *Phys. Rev. B*, 54:11169, 1996.

[31] G. Kresse and J. Furthmüller. Efficiency of ab-initio total energy calculations for metals and semiconductors using a plane wave basis set. *Comp. Mater. Sci.*, 6:15, 1996.

[32] P.E. Blöchl. Projector augmented-wave method. *Phys. Rev. B*, 50:17953, 1994.

[33] G. Kresse and D. Joubert. From ultrasoft pseudopotentials to the projector augmented-wave method. *Phys. Rev. B*, 59:1758, 1999.

[34] J. P. Perdew, K. Burke, and M. Ernzerhof. Generalized gradient approximation made simple. *Phys. Rev. Lett.*, 77:3865, 1996.

[35] J. P. Perdew, K. Burke, and M. Ernzerhof. Erratum: Generalized gradient approximation made simple. *Phys. Rev. Lett.*, 78:1396, 1997.

[36] T.A. Baker, C.M. Friend, and E. Kaxiras. Chlorine interaction with defects on the Au (111) surface: a first-principles theoretical investigation. *J. Chem. Phys.*, 129:104702, 2008.

[37] T.A. Baker, C.M. Friend, and E. Kaxiras. Effects of chlorine and oxygen coverage on the structure of the Au (111) surface. *J. Chem. Phys.*, 130:084701, 2009.

[38] A. Kiejna and B. I. Lundqvist. First-principles study of surface and subsurface o structures at al(111). *Phys. Rev. B*, 63:085405, Feb 2001.

[39] A. Kiejna and B.I. Lundqvist. Stability of oxygen adsorption sites and ultrathin aluminum oxide films on al(111). *Surface Science*, 504:1–10, 2002.

[40] A. Benali. *Étude ab initio d'alliages AlCu: phénomènes de ségrégation et modification de la réactivité de surface vis-à-vis de l'oxygène.* PhD thesis, École doctorale Science de la Matière, Toulouse, 2010.

[41] W.B. Pearson, I.D. Brown, and A.Mc.L. Mathieson. *Structure Reports*, 27, 1962.